AGU PUBLICATIONS

Geophysical Research Letters

RESEARCH LETTER
10.1002/2017GL076123

Key Points:
- Satellite observations of stratospheric gravity waves in 2002–2016 have been matched with a global tropical cyclone data set
- Stratospheric gravity wave activity was found to be statistically associated with the intensification of tropical cyclones
- Observations of stratospheric gravity waves above obscuring tropospheric clouds may be used as an indicator of storm intensification

Correspondence to:
X. Wu,
xu.wu@fz-juelich.de

Citation:
Hoffmann, L., Wu, X., & Alexander, M. J. (2018). Satellite observations of stratospheric gravity waves associated with the intensification of tropical cyclones. *Geophysical Research Letters*, *45*, 1692–1700. https://doi.org/10.1002/2017GL076123

Received 20 OCT 2017
Accepted 29 JAN 2018
Accepted article online 5 FEB 2018
Published online 12 FEB 2018

Satellite Observations of Stratospheric Gravity Waves Associated With the Intensification of Tropical Cyclones

Lars Hoffmann[1], **Xue Wu**[1,2], **and M. Joan Alexander**[3]

[1]Jülich Supercomputing Centre, Forschungszentrum Jülich, Jülich, Germany, [2]Institute of Atmospheric Physics, Chinese Academy of Sciences, Beijing, China, [3]NorthWest Research Associates, CoRA Office, Boulder, CO, USA

Abstract Forecasting the intensity of tropical cyclones is a challenging problem. Rapid intensification is often preceded by the formation of "hot towers" near the eyewall. Driven by strong release of latent heat, hot towers are high-reaching tropical cumulonimbus clouds that penetrate the tropopause. Hot towers are a potentially important source of stratospheric gravity waves. Using 13.5 years (2002–2016) of Atmospheric Infrared Sounder observations of stratospheric gravity waves and tropical cyclone data from the International Best Track Archive for Climate Stewardship, we found empirical evidence that stratospheric gravity wave activity is associated with the intensification of tropical cyclones. The Atmospheric Infrared Sounder and International Best Track Archive for Climate Stewardship data showed that strong gravity wave events occurred about twice as often for tropical cyclone intensification compared to storm weakening. Observations of stratospheric gravity waves, which are not affected by obscuring tropospheric clouds, may become an important future indicator of storm intensification.

1. Introduction

Tropical cyclones (TCs) are extreme meteorological events that encompass numerous natural hazards, such as strong winds, heavy rain, flooding, and storm surges, which subsequently lead to the destruction of infrastructure and endanger human life. Better knowledge about the track and intensity of TCs will help to make more informed decisions on actions to reduce loss of lives and property. In recent years, significant improvements have been made in track forecasting (Rappaport et al., 2009), but only modest improvements have been made in intensity forecasting (DeMaria et al., 2014). In particular, forecasting the rapid intensification of TCs is still a scientific challenge (DeMaria et al., 2014; Emanuel, 2017). Hurricane Joaquin during the 2015 Atlantic hurricane season is a primary example of the difficulties in predicting TC intensity. Joaquin was the strongest October hurricane in the Bahamas since 1866 and the strongest Atlantic hurricane of nontropical origin in the satellite era (since the 1960s). Joaquin devastated districts of the Bahamas, parts of the Greater Antilles, and Bermuda, killing 34 people and causing 200 million U.S. dollars in damages. The official forecast intensity errors for Joaquin were greater than the mean official errors for the previous 5 year period at all forecast times, and the error was largest during the unexpected rapid intensification phase (Berg, 2016).

TC-induced gravity waves (GWs) have been widely studied with model simulations, satellite, and ground-based observations, as well as reanalysis data (Chen et al., 2012; Chane Ming et al., 2010, 2014; Kuester et al., 2008; Kim et al., 2009; Miller et al., 2015; Nolan & Zhang, 2017; Wu et al., 2015; Yue et al., 2014). Typical characteristics, namely, the vertical and horizontal wavelength, period, and propagation direction have been assessed. The characteristics of GWs vary remarkably as the intensity of the TCs changes, reflecting variations in latent heat released by TCs. Observational and model results have shown that larger amplitude GWs develop when convection intensifies and deepens (Alexander et al., 2000; Beres et al., 2002, 2004; Lane et al., 2001), and a TC case study found that GWs were more intense during intensification (Chane Ming et al., 2014). Clusters of deep convection and hot towers may typically form several hours prior to TC rapid intensification (Hendricks et al., 2004; Simpson et al., 1998). Short horizontal and long vertical wavelength GWs emerging from the hot towers may need less than an hour to propagate into the stratosphere (Fritts & Alexander, 2003; Yue et al., 2013, 2014). Considering the timing, variations in stratospheric GWs signals may potentially be used as a proxy or indicator for the evolution of TC intensity. This may be particularly useful if direct observations of TC intensity changes are not available, for example, due to overlying cirrus in the line of sight of a satellite instrument.

In this study we provide observational evidence for previous model-inferred relationships between stratospheric GW activity and intensification of TCs, based on a case study for Hurricane Joaquin and a statistical analysis based on a long-term collection of satellite observations. The Atmospheric Infrared Sounder (AIRS) (Aumann et al., 2003; Chahine et al., 2006) aboard NASA's Aqua satellite has provided global high-resolution observations of stratospheric GWs since September 2002. A particular advantage of satellite observations over ground-based observing systems is that they provide views on stratospheric GWs from above the obscuring clouds. Furthermore, satellites provide the advantage of synoptic-scale observations when ground-based instruments do not. Finally, satellites give coverage of TCs in remote ocean regions that ground-based measurements cannot reach. AIRS data have been used successfully to characterize GWs from various sources (Alexander & Barnet, 2007; Gong et al., 2012; Hoffmann & Alexander, 2010; Hoffmann et al., 2013, 2014; Wu et al., 2015; Yue et al., 2013, 2014). By matching snapshots of GW observations from AIRS swaths with TC data from the International Best Track Archive for Climate Stewardship (IBTrACS) (Knapp et al., 2010), a large data set of GW activity for TC cases became available for investigating the relationship between GW activity and TC intensity in this study.

In section 2 we introduce the TC track and intensity data set, the AIRS observations of stratospheric GWs, and the meteorological reanalysis used to study TC-induced GW activity. The case study for Hurricane Joaquin and the statistical analysis for 13.5 years of AIRS observations are presented in section 3. Finally, our conclusions are summarized in section 4.

2. Data and Methods

2.1. TC Track and Intensity Estimates

In this study we analyzed TC track and intensity estimates from the IBTrACS (Knapp et al., 2010). These data were compiled from Regional Specialized Meteorological Centers within World Meteorological Organization (WMO), as well as from other national agencies, which compile and archive TC track data individually. Kruk et al. (2010) and Knapp et al. (2010) describe the procedure and issues involved in combining the data from the different centers into the IBTrACS data set. The first step in merging is the identification of individual storms in the different data sets, which may be particularly difficult for weak storms, with the center of circulation being difficult to diagnose or in the rare case that two storms merge. The second step is combining the intensity estimates. IBTrACS reports 6-hourly summary statistics such as the mean of the minimum sea level pressure (MSLP) and the 10 min maximum sustained wind (MSW) as intensity estimates of TC activity. Here we use version 3 (revision 9) of the IBTrACS-WMO data set, providing storm data for the time period from January 1848 to March 2016. We make use of data from September 2002 onward.

From the IBTrACS data we calculated the MSW temporal derivative as a measure for TC intensification or weakening, which we simply refer to as "intensity change" below. We considered MSW rather than MSLP as a primary measure of TC intensity, because MSW is typically used to rank TCs on different intensity scales. We calculated the intensity change linearly, using the 6-hourly IBTrACS data at the synoptic time steps before and after an AIRS observation. For instance, if the AIRS observations occurred at 09:00 UTC, we used IBTrACS data at 06:00 and 12:00 UTC to calculate intensity change. Some uncertainties are involved with the calculation of intensity change. First, based on a total of 12,874 data points extracted for the time period from September 2002 to March 2016, we found that MSW data are missing in about 15% of the cases, in particular toward the beginning or end of the tracks. Second, some centers provide MSW data only at discrete levels of 5 knots (about 2.6 m/s). Considering that IBTrACS data are provided only every 6 h, intensity change is partially measured at a relatively coarse level.

2.2. AIRS Observations of Stratospheric GWs

We used satellite observations from the AIRS (Aumann et al., 2003; Chahine et al., 2006) along the hurricane tracks to detect stratospheric GW activity. AIRS is one of six instruments aboard NASA's Aqua satellite (launched May 2002), which operates in a Sun-synchronous, nearly polar low Earth orbit with equator crossings at 01:30 and 13:30 local time. AIRS has been measuring about 2.9 million infrared radiance spectra per day in an across-track scanning geometry since September 2002. Following the approach of Hoffmann and Alexander (2010) and Hoffmann et al. (2013, 2014), information on stratospheric GWs were extracted from spectral mean radiance measurements in the 4.3 μm CO_2 waveband. The vertical coverage of the measurements is characterized by the temperature kernel functions of the AIRS 4.3 μm channels considered here. The spectral mean kernel function shows a broad maximum around 30–40 km altitude and has full width at

half maximum of about 25 km. Sensitivity tests show that GWs with vertical wavelengths longer than about 10–15 km can be detected from the measurements (Hoffmann & Alexander, 2010; Hoffmann et al., 2014). A detrending procedure for background removal was applied to the 4.3 μm brightness temperature (BT) measurements to extract GW signals. The detrended BT perturbations are most sensitive to GWs with horizontal wavelengths in the range of 30–700 km. Measurement noise of the 4.3 μm BTs is in the range of 0.06–0.12 K at typical scene temperatures of 235–250 K in the tropics. The AIRS 4.3 μm BT variances shown in this paper have been corrected for noise by subtracting a noise estimate based on the currently observed scene temperature. A distinct advantage of AIRS is that it facilitates simultaneous detections of clouds and storms via radiance measurements in the 8.1 μm spectral window region (Aumann et al., 2006).

We developed a simple algorithm to match the AIRS and IBTrACS data. For each ascending and descending section of the AIRS/Aqua orbits we stepped along the footprints of one of the center tracks of AIRS. Using the measurement time of the footprint, we interpolated the exact position of each storm present at the time using the 6-hourly IBTrACS data. Next, we found the minimum distance between the storm positions and the AIRS footprints. If the minimum distance was less than 890 km, that is, half the ground distance covered by the AIRS scans, we considered this to be a match. Analyzing the time period from September 2002 (beginning of the AIRS measurements) to March 2016 (end of the IBTrACS database), we found 12,874 matches of AIRS/Aqua overpasses and TC tracks. These matches covered a total of 1,221 storms. Most matches (a total of 39) of a single storm were found for TC Hondo during the 2007/2008 South-West Indian Ocean cyclone season. More than 614 storms had at least 10 AIRS/Aqua overpasses. Only 17 storms had just a single match. From a visual inspection of GW patterns in AIRS 4.3 μm BT perturbations maps for the 50 strongest GW events found in the AIRS/IBTrACS record, we conclude that the simple matching algorithm works quite well in detecting TC-induced GW events, with a success rate of at least 80–90%. In some cases it is difficult to differentiate between TC-induced GWs and GWs from other sources.

2.3. Stratospheric Background Winds From Meteorological Reanalysis

The third data set considered here is the Modern-Era Retrospective analysis for Research and Applications, Version 2 (MERRA-2) (Bosilovich et al., 2015). In particular, we used 3-hourly zonal and meridional winds to estimate the mean horizontal wind speed at the 3 hPa level (about 40 km) for $1,000 \times 1,000$ km^2 boxes centered on each AIRS/IBTrACS match. The 3 hPa background wind speeds at the AIRS observational level were used to assess and mitigate the impacts of critical-level wind filtering (Alexander, 1998; Fritts & Alexander, 2003; Taylor et al., 1993) and the observational filtering effect (Alexander & Barnet, 2007; Gong et al., 2012; Hoffmann et al., 2016). The GW dispersion relation ties vertical and horizontal wavelengths to the background winds. Strong background winds cause Doppler shifting of GWs toward high-intrinsic phase speeds and long vertical wavelengths. As AIRS is only capable of observing GWs with vertical wavelengths longer than about 10–15 km, this implies that significant stratospheric background winds must be present in order for AIRS to be able to observe GWs. Note that strong background winds cause asymmetry in observed wave patterns, with waves propagating upstream being shifted to longer vertical wavelengths and waves propagating downstream being shifted to shorter vertical wavelengths. As a consequence, wave patterns from convective and TC sources typically appear as semicircles in AIRS observations.

Inspecting the distribution of the AIRS 4.3 μm BT variances with respect to the 3 hPa background winds for all the matches, we empirically found that a minimum wind speed of about 20 m/s is required in order for AIRS to be able to see GW activity related to the TCs. In our statistical analysis we filtered out all the AIRS/IBTrACS matches with 3 hPa wind speeds below 20 m/s. A large fraction of matches is removed by this filter, between 38% in the tropics (25°S–25°N) and 52% in the extratropics, but these are all data points where AIRS is actually not able to provide any real information on GW activity since 4.3 μm BT variances are close to zero in these cases. The filtering criterion does not remove any strong GW peak events.

As the MERRA-2 3 hPa wind speeds are an important source of a priori information regarding the expected propagation characteristics and observability of the TC-induced GWs, we reviewed the literature regarding their accuracy. Most studies found that the MERRA-2 stratospheric winds are in good agreement with other global reanalyses and observations (Bosilovich et al., 2015; Coy et al., 2016; Long et al., 2017). Considering this, it seems acceptable to use MERRA-2 3 hPa wind speeds to assess the impact of the AIRS observational filter, as our application; that is, the threshold criterion on the wind speed does not critically depend on the absolute accuracy of the data.

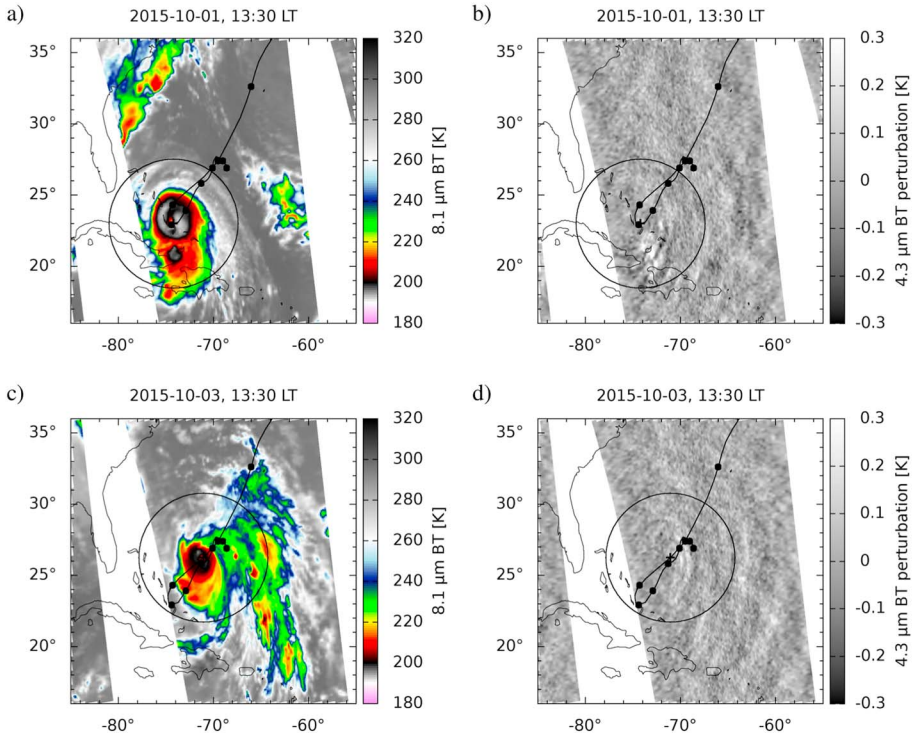

Figure 1. AIRS observations of Hurricane Joaquin on 1 and 3 October 2015. See plot titles for local time of AIRS/Aqua overpasses. (a, c) The 8.1 μm BT maps show cloud patterns associated with the hurricane and (b, d) the 4.3 μm BT perturbations maps show stratospheric GW patterns. The black curve indicates the IBTrACS best estimate of the hurricane track, with positions at 00:00 UTC marked by dots. The large black circle indicates the area used to detect GW signals.

3. Results

3.1. Case Study on Hurricane Joaquin

In this section we present a case study on Hurricane Joaquin showing links between stratospheric GW and TC activities. The synoptic history of Joaquin is summarized in the U.S. National Hurricane Center Tropical Cyclone Report by Berg (2016). Joaquin was the tenth named storm, third hurricane, and second major hurricane of the 2015 Atlantic hurricane season. It developed from a nontropical low into a tropical depression on 28 September, a tropical storm on 29 September, and a hurricane on 30 September. During that time, Joaquin slowly drifted southwestward toward very warm waters (30°C) near the Bahamas. It reached Category 4 major hurricane strength on 1 October. A middle- and upper-level trough over the eastern United States caused Joaquin to slow down even further and make a hairpin turn toward northeast. Following intermediate weakening, abrupt reintensification occurred on 3 October, when Joaquin reached a MSLP of 934 hPa and a MSW of 69 m/s, just short of Category 5 strength. Finally, increasing wind shear eroded the eyewall and Joaquin lost its status as a major hurricane on 4 October.

Figure 1 shows 8.1 and 4.3 μm BT data from AIRS overpasses over Hurricane Joaquin on 1 and 3 October 2015, which is when TC intensity was close to its maximum. The cloud patterns of the hurricane are easily identified in 8.1 μm BT maps. The patterns on 1 October are particularly complex, because they show the presence of a smaller convective region with minimum cloud top temperatures of about 190–195 K near 21°N, 74°W, just south of Joaquin's eye. The cloud maps illustrate that the AIRS/IBTrACS matching algorithm is working quite well, as the position of the match is coinciding with the eye of the hurricane within 20–30 km. The AIRS 4.3 μm BT perturbation maps show stratospheric GW patterns associated with the hurricane for both overpasses. The waves are propagating away from the center of the hurricane toward southeast on 1 October and east on 3 October. The wave propagation is predominantly upstream as MERRA-2 shows southeasterly winds at 3 hPa in the region covered by the waves on both days. We would expect to mostly see waves propagating upstream with AIRS, because wave refraction leads to longer vertical wavelengths in this case and the observational filtering effect (Alexander & Barnet, 2007). From the maps we estimated horizontal wavelengths in the range

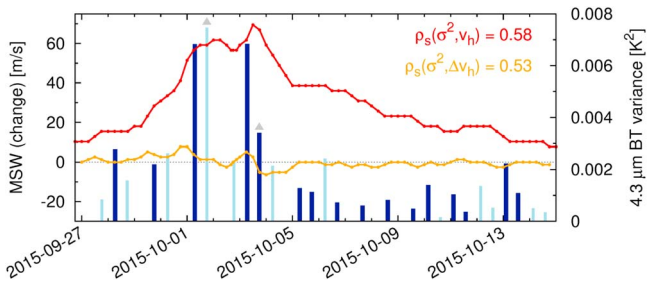

Figure 2. Time series of intensity (maximum sustained wind v_h, red, m/s) and intensity change (Δv_h, orange, m/s/(6 h)) of Hurricane Joaquin from the IBTrACS data set. Bars show detrended and noise-corrected 4.3 μm BT variances σ^2 from AIRS overpasses with good coverage (calculation based on ≥1,000 footprints; dark blue) or moderate coverage (calculation based on <1,000 footprints; light blue). Gray triangles indicate overpasses shown in Figure 1. $\rho_s(\sigma^2, v_h)$ and $\rho_s(\sigma^2, \Delta v_h)$ are the rank-order correlation coefficients between GW variances and intensity or intensity change, respectively.

of 90–100 km. Vertical wavelengths are at least 10–15 km due to the observational filtering effect, or even larger, considering the depth of the cloud and heating. GW ray tracing calculations for a number of convective storms conducted by Yue et al. (2013, 2014) suggest that waves with these characteristics propagate quickly up to stratospheric height levels of 30–40 km, typically within 20–60 min propagation time and 100–500 km horizontal propagation distance.

Figure 2 shows time series of intensity and intensity change from the 6-hourly IBTrACS data set as well as detrended and noise-corrected 4.3 μm BT variances from 28 overpasses of AIRS/Aqua over Hurricane Joaquin. During the hurricane's most intense phase on 1–3 October, the AIRS data set showed three GW events with variances as large as 6.8×10^{-3} to 7.4×10^{-3} K^2. These variances may appear to be small, but it needs to be taken into account that the wave patterns cover only a small part within the 500 km search radius that we are analyzing (see Figure 1). Maximum 4.3 μm BT perturbations for the three events are as large as ±0.6 K, which is exceeding AIRS noise levels by a factor of 5–10. These three peak events in wave activity are associated with positive intensity change. Two of them are associated with rapid intensification as MSW change exceeds levels of 15.4 m/s/(24 h), which is the definition of rapid intensification used by the National Hurricane Center. A number of smaller wave events associated with increasing intensity is also found on 28–30 September.

Considering the full time series for Hurricane Joaquin, we found Spearman rank-order correlation coefficients ρ_s between intensity v_h or intensity change Δv_h and GW variances σ^2 of $\rho_s(\sigma^2, v_h) = 0.58$ and $\rho_s(\sigma^2, \Delta v_h) = 0.53$, respectively. This indicates a "moderate" level of correlation. Mean correlation coefficients based on an analysis of time series of 615 storms having at least 10 satellite overpasses are $\rho_s(\sigma^2, v_h) = 0.19 \pm 0.35$ and $\rho_s(\sigma^2, \Delta v_h) = 0.10 \pm 0.33$, which is a "weak" or "very weak" correlation, respectively. Joaquin is a good example to demonstrate correlations between TC intensity and GW activity. We attribute the fact that average correlations are lower to limitations of the observations and meteorological variability of the background conditions, both of which will be discussed in more detail in the remainder of this paper.

3.2. Statistical Analysis of 2002–2016 Observations

Figure 3a shows a map of the AIRS/IBTrACS matches during September 2002 to March 2016, with GW peak events being shown on top. The largest number and most intense GW peak events are found over the Southern Indian Ocean and the Southern Pacific around 10 to 30°S. In the Northern Hemisphere variances are usually lower, with more intense events being found over the Western Pacific compared with the other ocean basins. For reference, Figure 3b is showing two of the factors that influence the distribution of the observed GW events. A direct comparison of the spatial patterns of GW variances and MSWs shown in Figure 3 suggests that both are correlated. However, a notable exception occurs in the Northern Hemisphere. Although there are a number of storms over the Eastern Pacific and North Atlantic with MSWs being larger than those found over the Western Pacific, wave activity maximizes over the Western Pacific. This discrepancy between the basins might be attributed to differences in occurrence frequencies of TCs. Knapp et al. (2010) found that there are typically up to 30 storms per decade over the Western Pacific but only 20 over the Eastern Pacific and 10 over the North Atlantic, implying that the largest chance for observing TC-induced GW events is over the Western Pacific. Another important factor to consider is the AIRS observational filtering effect. Mean 3 hPa wind speeds from MERRA-2 during the TC seasons are larger in the Southern Hemisphere (about 30 m/s around 10–25°S during November to March) than in the Northern Hemisphere (about 20 m/s around 15–20°N during June to October). This may explain the asymmetry between the hemispheres as AIRS has a better chance to observe GWs with longer vertical wavelengths in the Southern Hemisphere due to the stronger stratospheric background winds. GWs with short vertical wavelengths from the TC sources might be present in the Northern Hemisphere, but AIRS would have low chance to observe them.

Figure 4 presents the results of a statistical analysis of GW and TC activities. In total, there were 4,162 AIRS/IBTrACS matches for which MSW data are available and which passed the 3 hPa wind filtering criterion. About 1,000 events had a variance larger than 0.015 K^2 and about 100 events had a variance larger than 0.08 K^2 (Figure 4a). These variances are smaller than those associated with AIRS observations of GWs from

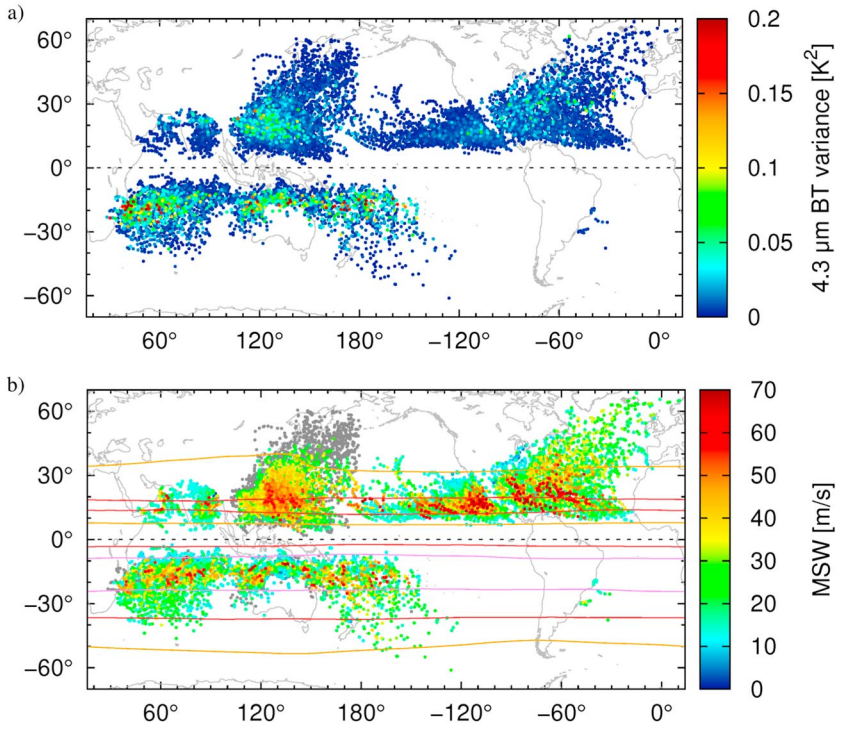

Figure 3. Matches of IBTrACS TC tracks and AIRS/Aqua overpasses during September 2002 to March 2016. (a) Color coding of symbols indicates detrended and noise-corrected 4.3 μm BT variance as measured by AIRS. Data points with largest variances appear on top. (b) Color coding of symbols indicates TC intensity. Data points with largest MSW appear on top. Gray color is used for missing data. Contour lines show 3 hPa mean zonal winds from MERRA-2 at levels of −10 m/s (orange), −20 m/s (red), and −30 m/s (purple) for June to October in the Northern Hemisphere and November to March in the Southern Hemisphere.

other sources such as mountain waves (e.g., Hoffmann, Grimsdell, et al., 2016), possibly due to the short vertical wavelengths of GWs sometimes emitted from TC sources (about 3–12 km in the troposphere and lower stratosphere) (Kim et al., 2009; Kuester et al., 2008; Wu et al., 2015) and due to the weaker 3 hPa winds during the TC seasons compared with middle- and high-latitude winter conditions.

Figure 4a shows a clear discrepancy in the number of GW events with respect to intensity change, with more events being associated with positive intensity change (TC intensification) rather than negative intensity change (TC weakening). The separation between increasing and decreasing MSW events is particularly clear for the peak events. The normalized ratio of events is increasing from 1 at 0.005 K^2 to about 2 at 0.15 K^2 (Figure 4b). We normalized at a level of 0.005 K^2 to compensate for the high bias of the full sample and to exclude a large number of weak events with GW activity being close to zero. For large variance thresholds the statistical uncertainty of the ratios is steadily increasing as they are calculated from smaller numbers of events.

In addition, we found that the probability distribution function of GW events with respect to intensity change is skewed toward increasing MSWs, in particular for larger variance thresholds (Figure 4c). For a threshold of 0.15 K^2 about 34% of the GW events were associated with TC intensification, 14% of the GW events were associated with TC weakening, and 52% of the GW events had intensity changes less than ±1.3 m/s/(6 h).

We conducted several consistency and sensitivity tests showing that the results of the statistical analysis are robust.

1. Results are consistent if we use MSLP instead of MSW as a measure of TC intensity, that is, GW activity is predominantly associated with decreasing MSLP.
2. Varying the search radius to calculate the 4.3 μm BT variances from the AIRS observations between 350 and 700 km does not notably affect the results. Likewise, results are robust regarding changes of the time interval used to calculate intensity change from the IBTrACS data between 6, 12, and 18 h.

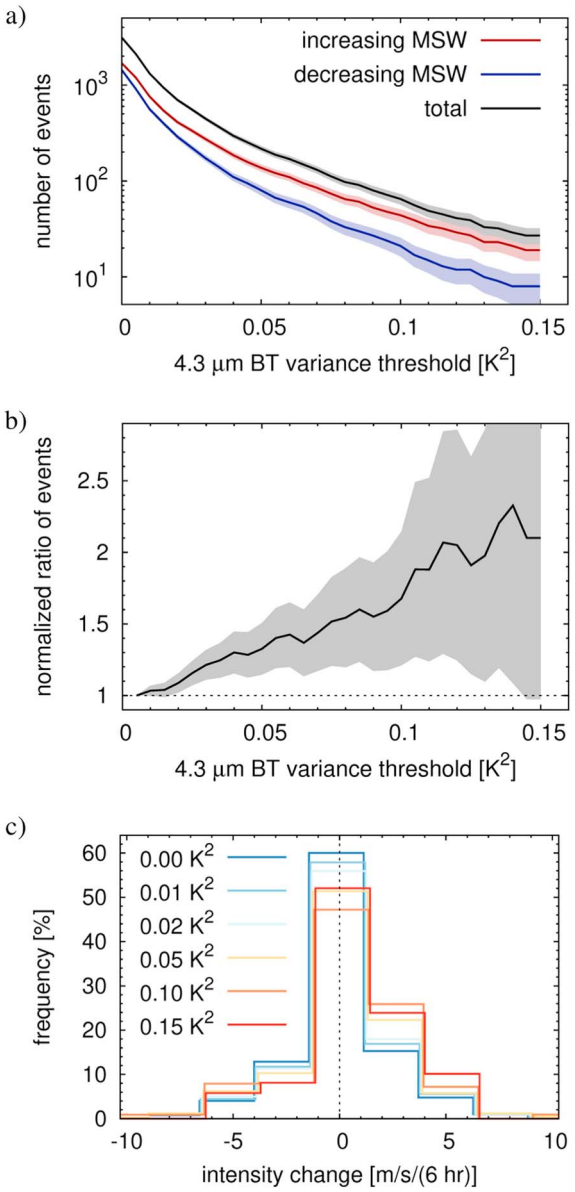

Figure 4. Statistical analysis of stratospheric GW events associated with TC activity. (a) Number of GW events associated with increasing or decreasing MSW for different minimum variance thresholds. (b) Ratios of events normalized with respect to the values for a variance threshold of 0.005 K^2. (c) Frequency distribution of events with respect to intensity change for selected variance thresholds. Plots show mean and standard deviation of the parameters from a bootstrapping analysis.

3. Results remain consistent, if we analyze events with eastward or westward propagating GWs separately. This test takes into account the changes of 3 hPa low- and middle-latitude winds from easterlies in summer to westerlies in winter, respectively.
4. Analyzing AIRS/Aqua overpasses from descending orbits (~01:30 LT) and ascending orbits (~13:30 LT) separately, we found that in both cases GW events are more likely to occur for TC intensification. However, the overall numbers of strong GW events are larger for nighttime than for daytime observations, which may be related to the diurnal cycle of TC intensity (Dunion et al., 2014).
5. Constraining the analysis to AIRS/Aqua overpasses with the TCs being closer to the center of the measurement track (match distances $\leq$ 600 km) improves coverage and horizontal resolution and reduces line-of-sight angle effects of the AIRS observations (Gong et al., 2012). Results remain robust, although the stronger constraint reduces the number of matches (by about 30%) and increases statistical uncertainty.
6. Statistical uncertainties have been assessed by means of a bootstrapping analysis (see Figure 4).

4. Conclusions

In this study we analyzed satellite observations of stratospheric GWs triggered by TCs. GW observations were obtained from the AIRS instrument aboard NASA's Aqua satellite, whereas best estimates of TC tracks and intensities were obtained from the IBTrACS compilation. In particular, we investigated if enhanced stratospheric GW activity can be related to intensification of TCs. As a prominent example, in a case study for Hurricane Joaquin over the North Atlantic around early October 2015 we found a Spearman rank-order correlation coefficient of 0.53 between GW variances and TC intensity change. However, TCs are a rather variable source of GWs and the propagation of GWs into the stratosphere is influenced by the background wind and stability profiles. The background winds also play an important role with respect to the AIRS observational filtering effect, that is, only GWs with vertical wavelengths longer than about 10–15 km can be observed. While modeling and observational analyses for individual case studies can help to better understand the physical mechanisms related to TC-induced GW excitation and propagation, we decided here to study the correlations between GW and TC activities mainly based on a statistical analysis. Our comprehensive analysis covers AIRS/Aqua overpasses of 1,221 storms during the years 2002–2016. The statistical analysis showed that about twice as many of the GW peak events are associated with intensification rather than weakening of TCs. The distribution of GW events with respect to TC intensity change is significantly skewed toward increasing MSW. The statistical analysis showed clearly that enhanced stratospheric GW activity is associated with the intensification of TCs.

Considering the evidence that stratospheric GW signals may be a proxy for the evolution of TC intensity, this study suggests that infrared imaging satellite observations could be a valuable asset for future work. Satellite instruments can observe stratospheric GWs clearly above obscuring clouds in the troposphere, and the observations may be used as an indicator of storm intensification. Nadir observations of GWs with short horizontal and long vertical wavelength are particularly useful, as these waves tend to propagate quickly from the TC sources in the troposphere into the stratosphere. However, the observational filtering effect is limiting the analysis to cases with strong stratospheric background wind speeds ($\geq$ 20 m/s at the 3 hPa level in this study). Another limitation of AIRS is that it provides only local snapshots of GW activity and clouds during two overpasses at 01:30 and 13:30 local time and does not cover the entire TC diurnal cycle. Furthermore, observations at low latitudes are restricted by the limited width of the AIRS scans, each covering 1,780 km of

ground distance, which causes data gaps between the neighboring measurement tracks. In addition, a more dense time sampling of TC intensity estimates than the 6-hourly IBTrACS data would be helpful to better assess the timing with respect to the GW events. A new satellite mission concept recently proposed, the Geostationary Hosted Observatory for Storm Tracking, would overcome those difficulties. The mission concept envisages a midinfrared imager hosted aboard a geostationary satellite positioned at 80°W longitude. The sensor would measure 4.26 and 4.40 μm thermal emissions with 3 km pixel size, 30 s refresh rate, and a signal-to-noise ratio improved by a factor of 5 compared with AIRS. Geostationary Hosted Observatory for Storm Tracking would facilitate persistent monitoring of stratospheric GW signatures and their relationship to the storms causing them at unprecedented spatial and temporal resolution for the North American continent and neighboring ocean regions.

Acknowledgments
AIRS and MERRA-2 data were obtained from the NASA Goddard Earth Sciences Data Information and Services Center (GES DISC) from their website at https://disc.gsfc.nasa.gov. IBTrACS data were obtained from the NOAA National Centers for Environmental Information from their website at https://www.ncdc.noaa.gov/ibtracs. We thank David S. Nolan for comments on an earlier draft of this manuscript. M. J. A. acknowledges support from the National Science Foundation grant 1519271. X. W. was supported by the National Natural Science Foundation of China under grant 41605023 and the International Postdoctoral Exchange Fellowship Program 2015 under grant 20151006.

References

Alexander, M. J. (1998). Interpretations of observed climatological patterns in stratospheric gravity wave variance. *Journal of Geophysical Research*, *103*(D8), 8627–8640.

Alexander, M. J., & Barnet, C. D. (2007). Using satellite observations to constrain gravity wave parameterizations for global models. *Journal of the Atmospheric Sciences*, *64*(5), 1652–1665.

Alexander, M. J., Beres, J. H., & Pfister, L. (2000). Tropical stratospheric gravity wave activity and relationships to clouds. *Journal of Geophysical Research*, *105*, 22,299–22,309.

Aumann, H. H., Chahine, M. T., Gautier, C., Goldberg, M. D., Kalnay, E., McMillin, L. M., … Susskind, J. (2003). AIRS/AMSU/HSB on the Aqua mission: Design, science objective, data products, and processing systems, *IEEE Transactions on Geoscience and Remote Sensing* (Vol. 41, pp. 253–264).

Aumann, H. H., Gregorich, D., & DeSouza-Machado, S. M. (2006). AIRS observations of deep convective clouds, *SPIE Photonics Conference* (pp. 6301–6320). San Diego: SPIE.

Beres, J. H., Alexander, M. J., & Holton, J. R. (2004). A method of specifying the gravity wave spectrum above convection based on latent heating properties and background wind. *Journal of Atmospheric Sciences*, *61*(3), 324–337.

Beres, J. H., Alexander, M. J., & Holton, J. R. (2002). Effects of tropospheric wind shear on the spectrum of convectively generated gravity waves. *Journal of the Atmospheric Sciences*, *59*(11), 1805–1824.

Berg, R. (2016). Tropical cyclone report: Hurricane Joaquin 2015 (Technical Report). Miami, FL: United States National Hurricane Center.

Bosilovich, M., Akella, S., Coy, L., Cullather, R., Draper, C., Gelaro, R., … Suarez, M. (2015). MERRA-2: Initial evaluation of the climate (*Technical Report Vol. 43*). Geenbelt, MD United States: NASA, Global Modeling and Data Assimilation, NASA/TM-2015-104606.

Chahine, M. T., Pagano, T. S., Aumann, H. H., Atlas, R., Barnet, C., Blaisdell, J., … Zhou, L. (2006). AIRS: Improving weather forecasting and providing new data on greenhouse gases. *Bulletin of the American Meteorological Society*, *87*(7), 911–926.

Chane Ming, F., Chen, Z., & Roux, F. (2010). Analysis of gravity-waves produced by intense tropical cyclones. *Annales Geophysicae*, *28*(2), 531–547. https://doi.org/10.5194/angeo-28-531-2010

Chane Ming, F., Ibrahim, C., Barthe, C., Jolivet, S., Keckhut, P., Liou, Y.-A., & Kuleshov, Y. (2014). Observation and a numerical study of gravity waves during tropical cyclone Ivan (2008). *Atmospheric Chemistry and Physics*, *14*(2), 641–658. https://doi.org/10.5194/acp-14-641-2014

Chen, D., Chen, Z., & Lü, D. (2012). Simulation of the stratospheric gravity waves generated by the Typhoon Matsa in 2005. *Science China Earth Sciences*, *55*(4), 602–610. https://doi.org/10.1007/s11430-011-4303-1

Coy, L., Wargan, K., Molod, A. M., McCarty, W. R., & Pawson, S. (2016). Structure and dynamics of the quasi-biennial oscillation in MERRA-2. *Journal of Climate*, *29*(14), 5339–5354.

DeMaria, M., Sampson, C. R., Knaff, J. A., & Musgrave, K. D. (2014). Is tropical cyclone intensity guidance improving? *Bulletin of the American Meteorological Society*, *95*(3), 387–398. https://doi.org/10.1175/BAMS-D-12-00240.1

Dunion, J. P., Thorncroft, C. D., & Velden, C. S. (2014). The tropical cyclone diurnal cycle of mature hurricanes. *Monthly Weather Review*, *142*(10), 3900–3919.

Emanuel, K. (2017). Will global warming make hurricane forecasting more difficult? *Bulletin of the American Meteorological Society*, *98*(3), 495–501. https://doi.org/10.1175/BAMS-D-16-0134.1

Fritts, D. C., & Alexander, M. J. (2003). Gravity wave dynamics and effects in the middle atmosphere. *Reviews of Geophysics*, *41*(1), 1003. https://doi.org/10.1029/2001RG000106

Gong, J., Wu, D. L., & Eckermann, S. D. (2012). Gravity wave variances and propagation derived from AIRS radiances. *Atmospheric Chemistry and Physics*, *12*(4), 1701–1720.

Hendricks, E. A., Montgomery, M. T., & Davis, C. A. (2004). The role of "vortical" hot towers in the formation of tropical cyclone Diana (1984). *Journal of the Atmospheric Sciences*, *61*(11), 1209–1232.

Hoffmann, L., & Alexander, M. J. (2010). Occurrence frequency of convective gravity waves during the North American thunderstorm season. *Journal of Geophysical Research*, *115*, D20111. https://doi.org/10.1029/2010JD014401

Hoffmann, L., Alexander, M. J., Clerbaux, C., Grimsdell, A. W., Meyer, C. I., Rößler, T., & Tournier, B. (2014). Intercomparison of stratospheric gravity wave observations with AIRS and IASI. *Atmospheric Measurement Techniques*, *7*(12), 4517–4537.

Hoffmann, L., Grimsdell, A. W., & Alexander, M. J. (2016). Stratospheric gravity waves at Southern Hemisphere orographic hotspots: 2003–2014 AIRS/Aqua observations. *Atmospheric Chemistry and Physics*, *16*(14), 9381–9397.

Hoffmann, L., Xue, X., & Alexander, M. J. (2013). A global view of stratospheric gravity wave hotspots located with Atmospheric Infrared Sounder observations. *Journal of Geophysical Research: Atmospheres*, *118*, 416–434. https://doi.org/10.1029/2012JD018658

Kim, S., Chun, H., & Wu, D. L. (2009). A study on stratospheric gravity waves generated by Typhoon Ewiniar: Numerical simulations and satellite observations. *Journal of Geophysical Research*, *114*, D22104. https://doi.org/10.1029/2009JD011971

Knapp, K. R., Kruk, M. C., Levinson, D. H., Diamond, H. J., & Neumann, C. J. (2010). The international best track archive for climate stewardship (IBTrACS) unifying tropical cyclone data. *Bulletin of the American Meteorological Society*, *91*(3), 363–376.

Kruk, M. C., Knapp, K. R., & Levinson, D. H. (2010). A technique for combining global tropical cyclone best track data. *Journal of Atmospheric and Oceanic Technology*, *27*(4), 680–692.

Kuester, M. A., Alexander, M. J., & Ray, E. A. (2008). A model study of gravity waves over Hurricane Humberto (2001). *Journal of Atmospheric Science*, *65*(10), 3231–3246.

Lane, T. P., Reeder, M. J., & Clark, T. L. (2001). Numerical modeling of gravity wave generation by deep tropical convection. *Journal of the Atmospheric Sciences*, *58*(10), 1249–1274.

Long, C. S., Fujiwara, M., Davis, S., Mitchell, D. M., & Wright, C. J. (2017). Climatology and interannual variability of dynamic variables in multiple reanalyses evaluated by the SPARC Reanalysis Intercomparison Project (S-RIP). *Atmospheric Chemistry and Physics*, *17*(23), 14,593–14,629. https://doi.org/10.5194/acp-17-14593-2017

Miller, S. D., Straka, W. C., Yue, J., Smith, S. M., Alexander, M. J., Hoffmann, L., … Partain, P. T. (2015). Upper atmospheric gravity wave details revealed in nightglow satellite imagery. *Proceedings of the National Academy of Sciences of the United States of America*, *112*(49), E6728—E6735. https://doi.org/10.1073/pnas.1508084112

Nolan, D. S., & Zhang, J. A. (2017). Spiral gravity waves radiating from tropical cyclones. *Geophysical Research Letters*, *44*, 3924–3931. https://doi.org/10.1002/2017GL073572

Rappaport, E. N., Franklin, J. L., Avila, L. A., Baig, S. R., Beven, J. L., Blake, E. S., … Tribble, A. N. (2009). Advances and challenges at the National Hurricane Center. *Weather and Forecasting*, *24*(2), 395–419. https://doi.org/10.1175/2008WAF2222128.1

Simpson, J., Halverson, J., Ferrier, B., Petersen, W., Simpson, R., Blakeslee, R., & Durden, S. (1998). On the role of "hot towers" in tropical cyclone formation. *Meteorology and Atmospheric Physics*, *67*(1), 15–35.

Taylor, M. J., Ryan, E. H., Tuan, T. F., & Edwards, R. (1993). Evidence of preferential directions for gravity wave propagation due to wind filtering in the middle atmosphere. *Journal of Geophysical Research*, *98*(A4), 6047–6057.

Wu, J. F., Xue, X. H., Hoffmann, L., Dou, X. K., Li, H. M., & Chen, T. D. (2015). A case study of typhoon-induced gravity waves and the orographic impacts related to Typhoon Mindulle (2004) over Taiwan. *Journal of Geophysical Research: Atmospheres*, *120*, 9193–9207. https://doi.org/10.1002/2015JD023517

Yue, J., Hoffmann, L., & Alexander, M. J. (2013). Simultaneous observations of convective gravity waves from a ground-based airglow imager and the AIRS satellite experiment. *Journal of Geophysical Research: Atmospheres*, *118*, 3178–3191. https://doi.org/10.1002/jgrd.50341

Yue, J., Miller, S. D., Hoffmann, L., & Straka, W. C. (2014). Stratospheric and mesospheric concentric gravity waves over tropical cyclone Mahasen: Joint AIRS and VIIRS satellite observations. *Journal of Atmospheric and Solar-Terrestrial Physics*, *119*, 83–90. https://doi.org/10.1016/j.jastp.2014.07.003

Yue, J., Thurairajah, B., Hoffmann, L., Alexander, M. J., Chandran, A., Taylor, M. J., … Bailey, S. M. (2014). Concentric gravity waves in polar mesospheric clouds from the Cloud Imaging and Particle Size experiment. *Journal of Geophysical Research: Atmospheres*, *119*, 5115–5127. https://doi.org/10.1002/2013JD021385